Detecting the Fermi surface nesting effect for the fermionic Dicke transition by trap-induced localization

Shi Chen and Yu Chen*

Graduate School of China Academy of Engineering Physics, Beijing 100193, China

(Received 4 April 2023; accepted 21 May 2024; published 12 July 2024)

Recently, the statistical effect of fermionic superradiance has been verified by a series of experiments both in free space and in a cavity. The Pauli blocking effect can be visualized by a $1/2$ scaling of the Dicke transition critical pumping strength against the particle number N_{at} for fermions in a trap. However, the evidence for the Fermi surface (FS) nesting effect, which manifests the enhancement of superradiance by Fermi statistics, is still missing. Here we report a scheme for detecting FS nesting with the help of the trap-induced localization on the trap edge. We find two scalings of the critical pumping strength as $N_{\mathrm{at}}^{-1.33}$ and $N_{\mathrm{at}}^{-0.67}$ for a moderate particle number when localization enters and the Pauli blocking scaling $1/3$ (two-dimensional case) in the $N_{\mathrm{at}} \to \infty$ limit is unaffected. Further, we find the scaling of the critical pumping strength against the particle number increases with the ratio between the recoil energy and the trap frequency in the direction orthogonal to the pumping direction E_R/ω_z. The scaling larger than 1 can be identified as a result of the Fermi surface nesting effect. Thus, we find a practical experimental scheme for visualizing the long-desired Fermi surface nesting effect with the help of trap-induced localization in a two-dimensional Fermi gas in a cavity.

DOI: 10.1103/PhysRevA.110.013312

I. INTRODUCTION

In recent decades, the developments in achieving strong coupling between atoms and light have led us to a new platform for studying nonequilibrium open quantum systems [1,2]. With these accumulations, the Dicke model, a typical model of strong interactions between atoms and light has finally been realized [3]. It ends the era of the Dicke transition being purely theoretical [4,5]. The Dicke transition manifests itself through the emergence of the steady-state superradiance together with a checkerboard density order in atoms [6]. The spontaneity of the self-organized crystalline is verified by the roton mode softening [7] and the critical behavior of the dynamical structure factor [8–10]. Exotic phases like density-ordered Mott insulators [11–14], as well as supersolid breaking U(1) symmetry and translation symmetry [15–17], are observed successively experimentally. Excited topics with the combinations of quantum many-body systems and the traditional presentation of an open quantum system—cavity QED (quantum electrodynamics)—have been enlightened following these new advances [18].

Besides the developments in the superradiance of Bose gases, there are also many interesting statistical effects in fermionic superradiance. The most prominent signature of a Dicke transition of degenerate Fermi gas is its density dependence, namely, the Fermi surface (FS) nesting effect and the Pauli blocking (PB) effect [19–21]. The FS nesting effect is due to the resonance between pairs of nested states on the FS whose momentum difference matches the cavity photon momentum. It results in a sharp decrease of the critical pumping strength at specific fillings. The PB effect, on the other hand, leads to a suppression of superradiance due to both of the momentum states connected by photon absorption being occupied. There are also further effects like a liquid-gas-like transition for p-band filling [19] and statistical crossover in interacting Fermi gases [22], etc. For a long time, these studies of statistical effects in fermionic superradiance have been only theoretical. In a recent experiment, a steady-state superradiance of fermions has been realized in a cavity for the first time [23,24]. A scaling law of the critical pumping strength (CPS) as $N_{\mathrm{at}}^{-1/2}$ against the particle number N_{at} at the large N_{at} limit is verified in a three-dimensional trapped fermion system [23]. This is in sharp contrast with the bosonic Dicke transition whose scaling law is N_{at}^{-1}. The PB effect in free-space superradiance is also verified thereafter [25–27]. Unfortunately, contrary to the well-established PB effect, the FS nesting effect, which shows the enhancement of superradiance by Fermi statistics is still not verified in experiment. The main difficulty is the presence of the trap makes density not well-defined.

In this article, we offer a method to identify the FS nesting effect for two-dimensional Fermi gases within a trap. We find that, when trap and optical lattice are both presented, there are localized states on the trap edge, which is similar to Stark localization. As is shown in Fig. 1(b), when the on-site energy difference outgoes the hopping strength on the trap edge, the particle is localized in the x direction. These localizations can result in one-dimensional fermion tubes on the trap edge, where the FS nesting effect is prominent. Phenomenologically, we find for different cavity detunings Δ_c, the CPS of the Dicke transition as a function of the particle number N_{at} falls into two typical functions. For small Δ_c, the CPS shows a scaling N_{at}^{-1} for small N_{at} and $N_{\mathrm{at}}^{-1/3}$ at a large N_{at} limit. There is no scaling faster than N_{at}^{-1}. Let us denote the scaling as $\varkappa$ for a CPS scaling law $N_{\mathrm{at}}^{-\varkappa}$ to simplify our description.

*Contact author: ychen@gscaep.ac.cn

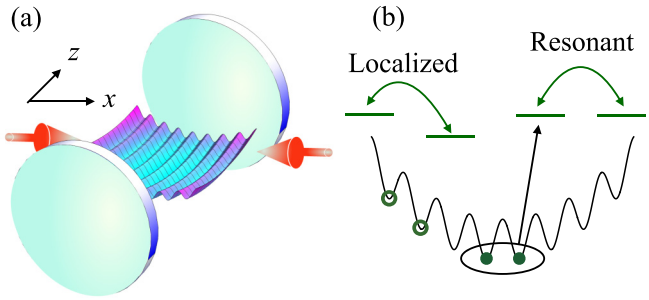

FIG. 1. In panel (a), we show the illustration of our setup. Two-dimensional Fermi gases are put into a cavity with a harmonic trap in the x and z directions. In panel (b), we show the mechanism for localization on the trap edge. At the bottom of the trap, fermions at neighbor sites are resonant, and thus the Bloch state is still a good approximation. On the edge of the trap, the on-site energy difference becomes larger than the hopping strength, which leads to localization.

For larger Δ_c, however, we find a scaling $\varkappa > 1$ ($\varkappa = 1.33$) in the intermediate particle number region. We also find a crossover between these two typical CPS functions, which is sharp within a very small window of Δ_c. In the same crossover Δ_c region, we find the eigenstate on the FS turns from an extended state to a localized state, which identifies the mechanism. Further, $\varkappa \to \infty$ in the $\omega_z/E_R \to 0$ limit at a specific $N_{\rm at}$ is obtained as a result of the FS nesting and this tendency is verified numerically. Therefore, the measurement of the critical pumping strength as a function of the particle number $N_{\rm at}$ for different cavity detunings Δ_c and different trap frequencies can help us to identify the FS nesting effect. We also stress that instead of being an obstacle, the presence of the trap is vital in detecting the FS nesting effect. Even more remarkably, we find the phenomenon is practical for experimental observation and can be very possibly observed in ^{6}Li atoms in a harmonic trap of $2\pi \times 260$ Hz frequency whose temperature is around $k_BT \sim 0.04E_R$ (E_R is the recoil energy of the ^{6}Li atom in typical optical lattice).

II. MODEL

We consider spinless fermions trapped inside a high-Q single-mode cavity within a harmonic trap ($\hbar = 1$ throughout),

$$\hat{H} = \hat{H}_{\rm at} - \Delta_c \hat{a}^\dagger \hat{a}, \tag{1}$$

$$\hat{H}_{\rm at} = \int d\mathbf{r} \hat{\psi}^\dagger(\mathbf{r})(\hat{H}_0 + \eta(\mathbf{r})(\hat{a}^\dagger + \hat{a}) + U_0(\mathbf{r})\hat{a}^\dagger\hat{a})\hat{\psi}(\mathbf{r}), \tag{2}$$

$$\hat{H}_0 = \frac{-\nabla^2}{2m} + V_P(\mathbf{r}) + \frac{1}{2}m\omega^2\mathbf{r}^2. \tag{3}$$

Here $\hat{a}$ is the annihilation operator of the cavity field, and $\hat{\psi}$ is an annihilation operator of fermionic atoms. Here $V_P(\mathbf{r}) = V_P \cos^2(k_0 x)$ is the optical lattice generated by the pumping field, $U_0(\mathbf{r}) = U_0 \cos^2(k_0 z)$ is the cavity field self-energy, and $\eta(\mathbf{r}) = \eta_0 \cos(k_0 x)\cos(k_0 z)$ is the interference between the pumping field and the cavity field. To be more specific, $V_P = \Omega_p^2/\Delta_a$, $U_0 = g_0^2/\Delta_a$, and $\eta_0 = g_0\Omega_p/\Delta_a$, where $\Delta_a = \omega_p - \omega_a$ is ac Stark shift (ω_a is the excited-state energy), and $\Delta_c = \omega_p - \omega_c$ is the cavity detuning. Here the cavity in consideration has a photon decay rate of κ. Ω_p is the strength of the pumping lasers, g_0 is the single-photon Rabi frequency of the cavity field, and k_0 is the wave number of the pumping field which is close to the wave number of the cavity field. The recoil energy is defined by $E_R \equiv k_0^2/2m$.

III. MEAN-FIELD THEORY

Since the cavity photon is lossy, the equation of the cavity photon field should follow the Lindblad equation,

$$i\partial_t \hat{a} = [\hat{a}, \hat{H}] + 2\kappa \mathcal{L}_{\hat{a}}\hat{a}, \tag{4}$$

where $\mathcal{L}_{\hat{a}}\hat{a} = \hat{a}^\dagger\hat{a}\hat{a} - \frac{1}{2}\{\hat{a}^\dagger\hat{a}, \hat{a}\}$ is the Lindblad operator on the cavity field operator $\hat{a}$. Assume that the cavity field is in a coherent state $|\alpha\rangle$, such that $\langle\alpha|\hat{a}|\alpha\rangle = \alpha$. Then the above equation can be written as

$$\partial_t \alpha = i[-\eta_0\Theta + (\Delta_c' + i\kappa)\alpha], \tag{5}$$

where the effective detuning $\Delta_c'(\alpha) = \Delta_c - \int d\mathbf{r} U(\mathbf{r})n(\mathbf{r})$ and $\Theta(\alpha) = \int d\mathbf{r} n(\mathbf{r})\eta(\mathbf{r})/\eta_0$. The fermionic density function is $n(r) \equiv \langle\hat{\psi}^\dagger(\mathbf{r})\hat{\psi}(\mathbf{r})\rangle = {\rm Tr}[\hat{\psi}^\dagger(\mathbf{r})\hat{\psi}(\mathbf{r})\hat{\rho}(t)]$. Here Tr is over the atom's Hilbert space and a coherent state of cavity field is assumed. Here we assume the steady-state density matrix of atoms is $\hat{\rho}_{\rm st} = e^{-\beta\hat{H}_{\rm at}(\alpha)}/Z$ [$Z = {\rm Tr}(e^{-\beta\hat{H}_{\rm at}(\alpha)})$], which is justified by a full dynamical handling by the Keldysh contour method. Here, $\hat{H}_{\rm at}(\alpha)$ is defined by replacing $\hat{a}$ in $\hat{H}_{\rm at}$ with α. In the steady state, $\partial\alpha/\partial t = 0$, we have

$$\alpha = \frac{\eta_0\Theta(\alpha)}{\Delta_c'(\alpha) + i\kappa}. \tag{6}$$

As α is complex, the above steady-state equation is indeed two equations. If we assume the Dicke transition is a second-order transition, then $\mathcal{B} = \int d\mathbf{r} U(\mathbf{r})n(\mathbf{r}) \approx U_0 N/2$. The phase of α is locked by κ. The other equation can be understood as a minimization of the free energy $\mathcal{F}_\alpha$,

$$\mathcal{F}_\alpha \equiv -\beta^{-1} \ln {\rm Tr}[e^{-\beta\hat{H}_{\rm at}(\alpha)}]. \tag{7}$$

One can check $\eta_0\Theta + \alpha \int d\mathbf{r} U(\mathbf{r})n(\mathbf{r}) = \partial\mathcal{F}_\alpha/\partial\alpha^*$. Then the steady-state equation becomes

$$\partial\mathcal{F}_\alpha/\partial\alpha^* - (\Delta_c + i\kappa)\alpha = 0. \tag{8}$$

Further in the second-order expansion of $\mathcal{F}_\alpha$, we can find $\mathcal{F}_\alpha = -\eta_0^2\chi(\alpha + \alpha^*)^2 + \mathcal{B}\alpha^*\alpha$, where $\chi = \int d\mathbf{r}d\mathbf{r}' \langle\delta n(\mathbf{r})\eta(\mathbf{r})\delta n(\mathbf{r}')\eta(\mathbf{r}')\rangle/\eta_0^2$ is the static structure factor, which characterizes the density fluctuation at momentum $\pm k_0\mathbf{e}_x + \pm k_0\mathbf{e}_z$:

$$\chi = \frac{1}{2\eta_0^2}\sum_{n,n'}\left|\int d\mathbf{r}\phi_n^*(\mathbf{r})\phi_{n'}(\mathbf{r})\eta(\mathbf{r})\right|^2 \frac{n_F(E_n) - n_F(E_n')}{E_{n'} - E_n}. \tag{9}$$

Here $\phi_n(\mathbf{r})$ is the eigenstate of $\hat{H}_0$, E_n is the corresponding eigenenergy of state $|n\rangle$, and $n_F(\epsilon) = 1/(e^{\beta(\epsilon-\mu)} + 1)$ is the Fermi distribution function. As it is known that the Dicke transition is a second-order transition [28], the critical pumping strength (CPS) is obtained on the condition that $\Delta_c' + 4\eta_0^2\chi\Delta_c'^2/(\Delta_c'^2 + \kappa^2) = 0$ for the second-order coefficient of

α in $\mathcal{F}_\alpha$ being zero. The CPS is

$$\left|\frac{V_P^{\rm cr}(N_{\rm at})}{E_R}\right| = \frac{-\left(\Delta_c'^2+\kappa^2\right)E_R}{4U_0\Delta_c'\chi(N_{\rm at})}. \tag{10}$$

In this paper, we focus on the scaling of $V_P^{\rm cr}$ over $N_{\rm at}$ to identify the statistical effect in fermionic superradiance transition at zero temperature.

IV. LOCALIZATION ON THE TRAP EDGE

In previous calculations for fermions in a trap, we have assumed that the fermions' states are more close to plane waves. However, on the edge of the trap, the interplay between the pumping lattice and the trap can lead to localization. Here we show the mechanism in a two-dimensional noninteracting fermion in a two-dimensional trap. Let us consider the Hamiltonian of atoms:

$$\hat{H}_0 = -\frac{\partial_x^2}{2m} + V_P(x) + \frac{m\omega_0^2}{2}x^2 - \frac{\partial_z^2}{2m} + \frac{m\omega_0^2}{2}z^2. \tag{11}$$

Assume the pumping strength is not small, we can construct $\hat{H}_0$ by the Wannier wave function. First we factorize out the eigenstate in the z direction and we label the state as $|j, n_z\rangle$, where j is the site index in the x direction and n_z is the quantum number of the harmonic trap in the z direction. $\phi_{n_z}(z)$ is the eigenstate of the harmonic trap, and its eigenenergy is $n_z\omega_0$. $\hbar = 1$. Here we assume $u_{1,k_x}(x)$ is the lowest-band Bloch wave function of $-\frac{\partial_x^2}{2m} + V_P(x)$; thus, $[-\frac{\partial_x^2}{2m} + V_P(x)]u_{1,k_x}(x) = \epsilon_{k_x}u_{1,k_x}(x)$. Then a Wannier basis can be constructed as

$$w_j(x) = \int dk_x e^{-ik_x jd}u_{1,k_x}(x), \tag{12}$$

where j is the site index, and $d = \frac{\pi}{k_0}$. Then we take the complete basis $\langle x, z|j, n_z\rangle = w_j(x)\phi_{n_z}(z)$ as our representation basis, the Hamiltonian $\hat{H}_0$ can be written as

$$\begin{aligned}\hat{H}_0 &= -\frac{\partial_x^2}{2m} + \frac{1}{2}m\omega^2x^2 + V_P\cos^2(k_0x) - \frac{\partial_z^2}{2m} + \frac{m\omega_0^2}{2}z^2 \\ &= \sum_{j,n_z;j',n_z'} |j', n_z'\rangle\langle j', n_z'|\hat{H}_0|j, n_z\rangle\langle j, n_z| \\ &= \sum_j \mu_j\,|j\rangle\,\langle j| + t\,|j\rangle\,\langle j+1| + t\,|j\rangle\,\langle j-1| + \cdots \\ &\quad + \sum_{n_z} n_z\omega_0|n_z\rangle\langle n_z|,\end{aligned} \tag{13}$$

where $t = \int dx w_i(x)[-\frac{\partial_x^2}{2m} + V_p\cos^2(k_0x)]w_{i+1}^*(x)$, and $\mu_i = \int dy|w_i(x)|^2\frac{1}{2}\omega^2x^2$. The omitted terms are next-to-nearest-neighbor hopping terms that are not explicitly shown in the formula.

One can check that when $|\mu_{j+1} - \mu_j| > t$, the eigenstate is localized because the resonance condition between sites is broken down. Here we employ the wave packet width to quantitatively characterize the localization degree of these eigenstates for different eigenenergies. The width of a state is defined as

$$\Delta(E_n) = \sqrt{\langle x^2\rangle_n - \langle x\rangle_n^2}, \tag{14}$$

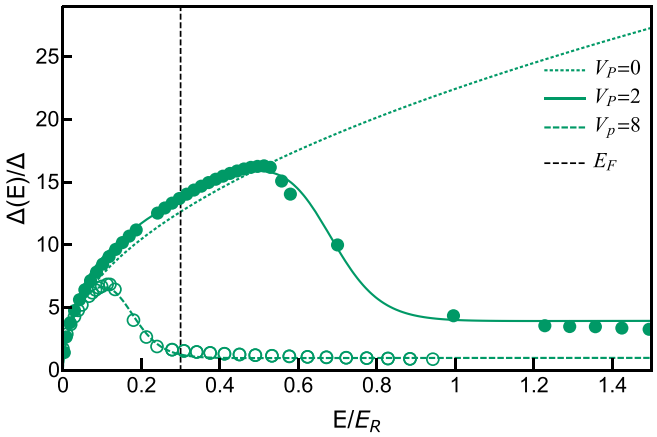

FIG. 2. The width $\Delta(E)$ of different eigenstates of $\hat{H}_y$ for different values of V_0. $\Delta = \frac{\pi}{k_0}$ is the lattice spacing. The black dashed line represents the typical Fermi energy in our setup.

where $\langle x^2\rangle_n = \int dx x^2|\phi_n(x)|^2$ and $\langle x\rangle_n = \int dx x|\phi_n(x)|^2$. In Fig. 2, we show $\Delta(E_n)$ as a function of the excitation energy E_n for different pumping lattice strengths for fixed trap frequency. A clear sign for the mobility edge is shown, and the high-energy states cannot be approximated as extended states. In the following, we explore the physical consequences of the trap-edge localization.

V. SCALING OF THE CRITICAL PUMPING STRENGTH

Following Eqs. (9) and (10), together with the calculation of eigenstate $|n\rangle = |n_x, n_z\rangle$, we can obtain the numerical result for $V_P^{\rm cr}$ for different values of Δ_c and particle numbers $N_{\rm at}$. Here we have fixed $\omega_x = \omega_z = E_R/50$. One can find when Δ_c' is larger the CPS is larger; thus the localization effect at the trap edge is larger. The numerical results for the CPS of the particle number $N_{\rm at}$ for different values of Δ_c' are given in Fig. 3(a). One can find for smaller Δ_c', the log-log plot of $V_P^{\rm cr}(N_{\rm at})$ up to a multiplier constant factor falls into one universal curve. The initial scaling of $V_P^{\rm cr}$ against $N_{\rm at}$ is -1, then it crosses over to -0.66 and finally it crosses over to -0.35 in the large $N_{\rm at}$ limit. The scaling reduction is due to the Pauli blocking effect. One can also find there are no scalings larger than 1, which means we only observe the suppression of superradiance due to the Fermi statistics. The situation suddenly changes when $\Delta_c' > 0.5$ MHz. We find due to localization on the trap edge, the CPS function $V_P^{\rm cr}(N_{\rm at})$ falls into a new universal curve. In this new universal curve, the initial small $N_{\rm at}$ scaling and the large particle number scaling are the same as those of the previous universal curve. Furthermore, a scaling being larger than 1 emerges around the middle range $N_{\rm at}$. This middle range $N_{\rm at}$ matches the fermion density for the FS nesting effect. We compared the crossover region of the universal critical pumping strength curve and the localization effect shown by the typical width of the wave function $\phi_{n_x}(x)$ at the Fermi level. We find these two regions coincide with each other. Here we define $L_{1.33}$ as the length of $V_P^{\rm cr}(N_{\rm at})$ whose particle number scaling is 1.33. Therefore, we conclude that the Pauli blocking scaling 0.34 is not affected by localization and a new scaling of 1.33 emerges due to the

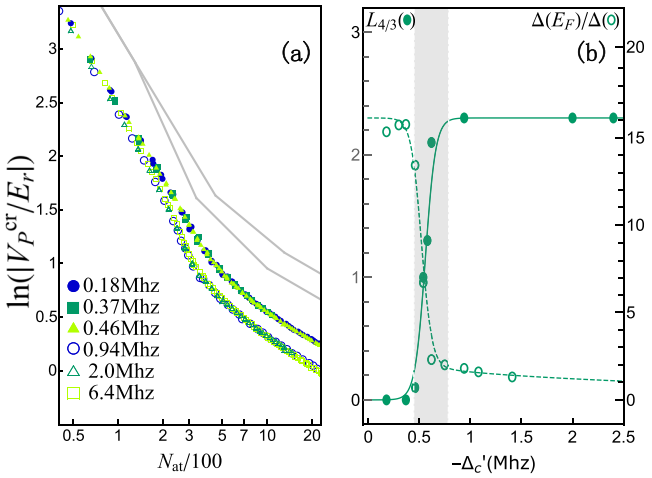

FIG. 3. We fix $\kappa = 1$ MHz and $U_0 = -100$ Hz. In panel (a), we show the critical pumping strength of the Dicke transition as a function of N_{at} for different values of Δ_c. In panel (b), the dashed line shows the packet width of state near the Fermi surface, and the solid line represents the length with a gradient of 1.33 in panel (a).

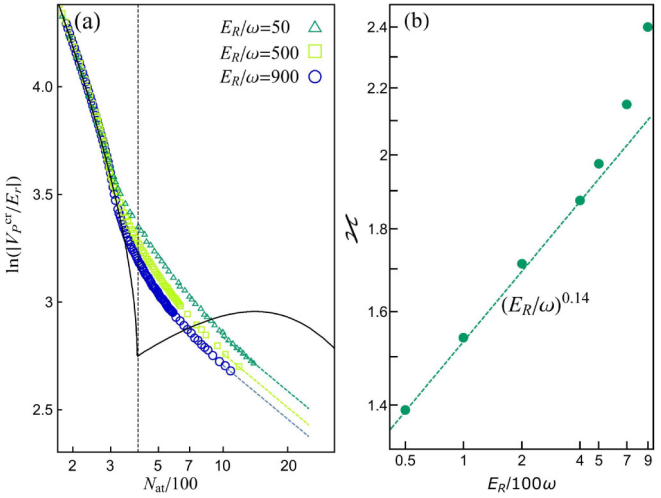

FIG. 4. In panel (a), we show the critical pumping strength as a function of the particle number for different ω_z/E_R. Δ_c is taken in the localized region. One can find that, when E_R/ω_z becomes bigger, the slope in the nesting region increases. The gray solid line is the theoretical prediction that we expect as the $E_R/\omega_z \to \infty$ limit of the universal critical pumping strength curve. In panel (b), we show the slope as a function of E_R/ω_z. The increase of the slope is found to be faster than the power law increasing. As a result, we expect $\varkappa_{\text{Nest}} \to \infty$ as $\omega_z/E_R \to 0$.

localization effect. Thus, we find the evidence of the FS nesting effect can be magnified by the localization effect induced by the trap.

To go further, we now present a theoretical effective theory to understand why the Pauli blocking effect is immune to the localization effect in the large N_{at} limit and whether the scaling 1.33 can be interpreted as the FS nesting effect. Before we give our analysis, we first give our conclusion. The predictions of our effective theory are (i) the large N_{at} limit of V_P^{cr} is $V_P^{cr} \propto N^{-1/3}$ and it is not changed by the localization effect, and (ii) there is a kink at some middle range N_{at}, and the CPS scaling of N_{at} becomes divergent before the kink in the $\omega_z \to 0$ limit. The second phenomenon is a signature of the FS nesting effect.

Now we present the assumptions of our effective theory. First of all, $\phi_{n_z}(z)$ is approximated by its large n_z asymptotic expression: $\phi_{n_z}(z) \sim \cos(\sqrt{(2n_z + 1/2)\omega_z}z)$ for even n_z and $\sin(\sqrt{(2n_z + 1/2)\omega_z}z)$ for odd n_z. Although the original approximation is only correct at the large n_z limit, here we take an approximation for every n_z. Furthermore, we drop the constant $1/2$ and employ $k_z^2 = 2n_z\omega_z$. Thus, $\sum_{n_z} = \int \frac{|k_z|}{m\omega_z} dk_z$ and $\phi_{n_z}(z) = \cos(k_z z)$ or $\sin(k_z z)$. Second, in the x direction, if $\phi_{n_x}(x)$ is localized at x_0, then $\phi_{n_x}(x) = \delta(x - x_0)$. If the wave function is not localized, we apply a local density approximation and $\phi_{n_x}(x)$ is characterized by both the position x_0 and the wave vector k_x. The eigenenergy is $\varepsilon_{x_0,k_x} = 2t \cos k_x + \frac{1}{2}\omega_x x_0^2$. Here we introduce x_{Mob} as the mobility edge in the x direction. For $x < x_{\text{Mob}}$, the wave function $\phi_{n_x}(x)$ is extended, and for $x > x_{\text{Mob}}$, the wave function is localized. $\sum_{n_x}$ is approximated as a phase space integral $\int dk_x dx_0$. With all these approximations, Eqs. (9) and (10) can be calculated analytically and we find $V_P^{cr} \propto N_{at}^{-1/3}$ at the large N_{at} limit irrelevant to the position of x_{Mob}. The detailed calculations are given in the Appendices [29] and the theoretical prediction is shown in Fig. 4(a) as the solid black curve. A kink at the FS nesting atom number can be observed.

Here we would like to add some comments on whether the localization in the x direction gives us one-dimensional tubes of fermions which can be automatically seen as several one-dimensional systems. A short answer is no. There are, in general, two reasons. One reason is that the density of states, especially the low-energy density of states, is modified by the harmonic trap. The second reason is the cavity-mode-induced off-diagonal terms between n_z and n_z' are not completely delta functions with momentum conservation like they are in free space. The broadening of the off-diagonal terms weakens the FS nesting signal as well. Because of these two reasons, we cannot treat the localized quasi-one-dimensional tubes as completely one-dimensional fermions. Thus, the final result is more like a dimension crossover between one-dimensional and two-dimensional systems.

Since the approximation in the z direction deviates from reality, we find the approximation is better when $E_R/\omega_z \gg 1$. Therefore, we expect the critical pumping strength scaling of N_{at} in the middle range N_{at} will increase when ω_z/E_R is decreasing. Thus, this prediction can be numerically checked by numerics. Interestingly, we find except for scaling around the Fermi surface nesting atom number, other scalings of the critical pumping strength are invariant for different values of ω_z. The scaling of the critical pumping strength $\ln(|V_P^{cr}/E_r|)/\ln N_{at}$ is increasing when ω_z is decreasing. We are restricted by the system size and the particle number in a numerical calculation; therefore, we can only prove that the scaling is increasing when ω_z becomes smaller. A finite-size scaling is carried out, and a divergent scaling is obtained in the $\omega_z \to 0$ limit. All of the present data analysis can be equally done for experimental data. These signatures in the critical pumping strength can then be identified as the FS nesting effect.

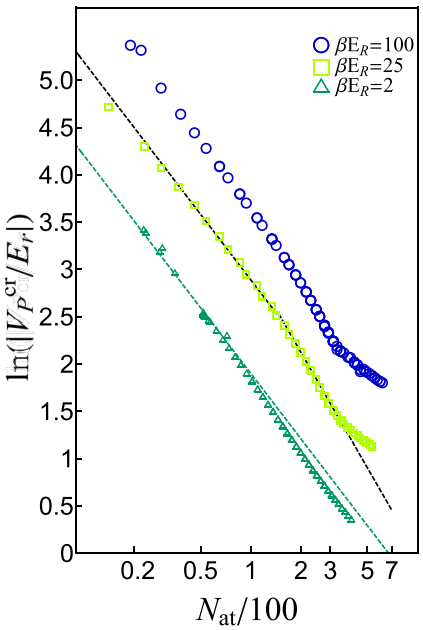

FIG. 5. The critical pumping strength $V_P^{\rm cr}$ as a function of the fermion atom number $N_{\rm at}$. The trap frequency is fixed at $E_R/\omega = 50$, $\Delta_c = -2\,\text{MHz}$, $U_0 = -100\,\text{Hz}$, and $\kappa = 1\,\text{MHz}$. The circle data are the lowest-temperature line where $k_BT/E_R = 0.01$. The square data are for the temperature $k_BT/E_R = 0.04$. The triangle data are the high-temperature data for $k_BT/E_R = 0.5$. For the temperature $k_BT/E_R = 0.04$, we can still see the signature for the FS nesting. However at high temperature, the slope kink in the critical pumping strength gradually disappears.

VI. FINITE-TEMPERATURE RESULT AND EXPERIMENTAL RELEVANCY

In the previous sections, we took an ideal situation to study to simplify the problem. Here we are going to give an analysis for experimental accessing. Here we suppose the fermion atom is ^{6}Li. The pumping laser's wavelength is taken as $\lambda_p = 1064$ nm. Then the recoil energy $E_R/\hbar$ can be obtained as $2\pi \times 2.9\,\text{kHz}$. The harmonic trap frequency is taken as $\omega_x = \omega_z = \omega_0 = 2\pi \times 290\,\text{Hz}$. Thus, we have $E_R/\hbar\omega = (h^2/2m\lambda_p^2)/\hbar\omega = 100$. The interacting strength between the atoms and light is taken as $U_0 = -100\,\text{Hz}$, $\kappa = 1\,\text{MHz}$, and the cavity detuning is taken as $\Delta_c = -2\,\text{MHz}$. Here we consider the $N_{\rm at}$ atoms are trapped in the two-dimensional harmonic trap at temperatures $k_BT/E_R \sim 0.01$, 0.04, and 0.5. The low-temperature k_BT/E_R is accessible. The $N_{\rm at}$ atoms range from 10 to 600. Under this setup, we can carry out the theoretical calculation by replacing the zero-temperature Fermi-Dirac distribution to finite-temperature distribution. The critical pumping strength as a function of atom in a ln-ln plot is shown in Fig. 5. From the critical pumping strength data of different temperatures, we find the slope kink in the critical pumping strength as the function of $N_{\rm at}$ gradually disappears. There is a clear signal for the slope being larger than 1 at the finite temperature $k_BT/E_R = 0.04$. Therefore, this phenomenon could very possibly be observed in the present setup of fermionic superradiance.

VII. CONCLUSION

To summarize, we find the Fermi surface nesting effect in the fermionic superradiant transition in a cavity can be verified with the help of trap-induced localization. We find when the harmonic trap depth is effectively changed, there are two typical curves for the superradiant transition critical pumping strength as a function of the particle number. For a shallow trap without the localization effect (x direction), there are no signs of FS nesting, and for a tight trap with the localization effect, there is a FS nesting signal which manifests as $\varkappa > 1$ for $\varkappa = \ln(|V_P^{\rm cr}/E_r|)/\ln N_{\rm at}$. We also verified the tendency for $\varkappa \to \infty$ in a limit when the trap frequency in the z direction becomes zero. We find the interplay between trap or localization and superradiance is quite interesting, and the statistical effect can be magnified and thus benefits the generation of superradiance.

ACKNOWLEDGMENTS

This work is supported by the National Key R&D Program of China (Grant No. 2022YFA1405300), the National Natural Science Foundation of China (Grants No. 12174358 and No. 11734010), the Beijing Natural Science Foundation (Grant No. Z180013), and the NSAF (Grant No. U2330401).

APPENDIX A: CALCULATION OF THE OFF-DIAGONAL MATRIX ELEMENT $\langle n|\cos(k_0z)|n'\rangle$ IN EQ. (8)

The transition matrix element $\langle n|\cos(k_0z)|n'\rangle = \int dz\phi_n^*(z)\phi_{n'}(z)\cos(k_0z)$, $\phi_{n'}(z)$, where $\phi_{n(n')}(z)$ is the eigenstate of the harmonic trap in the z direction. $\hat{H}_z|n\rangle = [-\partial_z^2/2m + (m\omega_z z^2)/2]\phi_n(z) = \omega_n^z\phi_n(z)$, $\omega_n^z = (n+1/2)\omega_z$, and $\hbar = 1$ is employed. Here we introduce

$$f_{nn'} = \langle n|e^{ik_0z}|n'\rangle, \tag{A1}$$

and then we can find that

$$\int dz\phi_n^*(z)\phi_{n'}(z)\cos(k_0z) = \int dz\phi_n^*(z)\phi_{n'}(z)\text{Re}(e^{ik_0z}) = \text{Re}(\langle n|e^{ik_0z}|n'\rangle) = \text{Re}(f_{nn'}). \tag{A2}$$

Since the transition element is just the real part of $f_{nn'}$, we focus on calculation of $f_{nn'}$ in the following. Here we present an algebraic method involving the annihilation and creation operators. Let us introduce $\hat{a} = \sqrt{\frac{m\omega_z}{2}}z + \sqrt{\frac{1}{2m\omega_z}}\partial_z$ and $\hat{a}^\dagger = \sqrt{\frac{m\omega_z}{2}}z - \sqrt{\frac{1}{2m\omega_z}}\partial_z$; then we have $z = \sqrt{\frac{1}{2m\omega_z}}(\hat{a}+\hat{a}^\dagger)$ and $\hat{H}_z = \omega_z(\hat{a}^\dagger\hat{a} + \frac{1}{2})$. Then eigenstate $|n\rangle = (\hat{a}^\dagger)^n/\sqrt{n!}|0\rangle$. We find

$$f_{nn'} = \langle n|e^{ik_0z}|n'\rangle = \frac{1}{\sqrt{n!n'!}}\langle 0|\hat{a}^n e^{i\frac{k_0}{\sqrt{2m\omega_z}}(\hat{a}+\hat{a}^\dagger)}(\hat{a}^\dagger)^{n'}|0\rangle. \tag{A3}$$

Let us introduce $\vartheta = k_0/\sqrt{2m\omega_z}$, and then we have

$$f_{nn'} = \langle n|\,e^{ik_0z}\,|n'\rangle = \frac{1}{\sqrt{n!n'!}}\langle 0|\hat{a}^n e^{i\vartheta(\hat{a}+\hat{a}^\dagger)}(\hat{a}^\dagger)^{n'}|0\rangle = \frac{1}{\sqrt{n!n'!}}\langle 0|e^{i\vartheta(\hat{a}+\hat{a}^\dagger)}e^{-i\vartheta(\hat{a}+\hat{a}^\dagger)}\hat{a}^n e^{i\vartheta(\hat{a}+\hat{a}^\dagger)}(\hat{a}^\dagger)^{n'}|0\rangle. \tag{A4}$$

Making use of the Baker-Hausdorff formula, we find

$$
\begin{aligned}
&e^{-i\vartheta(\hat{a}+\hat{a}^\dagger)}\hat{a}^n e^{i\vartheta(\hat{a}+\hat{a}^\dagger)} \\
&\quad = (e^{-i\vartheta(\hat{a}+\hat{a}^\dagger)}\hat{a}e^{i\vartheta(\hat{a}+\hat{a}^\dagger)})^n \\
&\quad = \left(\hat{a} - i\vartheta[\hat{a}+\hat{a}^\dagger,\hat{a}] + \sum_{\ell=2}^{\infty}\frac{(-i\vartheta)^\ell}{\ell!}[\ldots,[\hat{a}+\hat{a}^\dagger,\hat{a}],\ldots]\right)^n \\
&\quad = (\hat{a}+i\vartheta)^n. \qquad \text{(A5)}
\end{aligned}
$$

Therefore,

$$
\begin{aligned}
f_{nn'} &= \frac{1}{\sqrt{n!n'!}}\langle 0|e^{i\vartheta(\hat{a}+\hat{a}^\dagger)}(\hat{a}+i\vartheta)^n(\hat{a}^\dagger)^{n'}|0\rangle \\
&= \frac{1}{\sqrt{n!}}\langle 0|e^{i\vartheta(\hat{a}+\hat{a}^\dagger)}\sum_\ell C_n^\ell(i\vartheta)^{n-\ell}\hat{a}^\ell|n'\rangle. \qquad \text{(A6)}
\end{aligned}
$$

Here we assume $n \leqslant n'$, and then we have $\hat{a}^\ell|n'\rangle = (\sqrt{n'!/(n'-\ell)!})|n'-\ell\rangle$. Notice $e^{-i\vartheta(\hat{a}+\hat{a}^\dagger)}|0\rangle$ is a coherent state, denoted as $|-i\vartheta\rangle$; $\langle 0|e^{i\vartheta(\hat{a}+\hat{a}^\dagger)} = \langle -i\vartheta|$; and

$$
\begin{aligned}
f_{nn'} &= \frac{1}{\sqrt{n!}}\sum_\ell C_n^\ell(i\vartheta)^{n-\ell}\sqrt{\frac{n'!}{(n'-\ell)!}}\langle -i\vartheta|n-\ell\rangle \\
&= \frac{1}{\sqrt{n!}}\sum_\ell C_n^\ell(i\vartheta)^{n-\ell}\sqrt{\frac{n'!}{(n'-\ell)!}}\sqrt{\frac{1}{(n'-\ell)!}} \\
&\quad \times \langle -i\vartheta|(\hat{a}^\dagger)^{n'-\ell}|0\rangle \\
&= \frac{\sqrt{n'!}}{\sqrt{n!}}\sum_\ell C_n^\ell(i\vartheta)^{n-\ell}\frac{1}{(n'-\ell)!}((-i\vartheta)^*)^{n'-\ell}\langle -i\vartheta|0\rangle. \qquad \text{(A7)}
\end{aligned}
$$

In the last line of above equation, we have used $\langle -i\vartheta|\hat{a}^\dagger = (-i\vartheta)^*\langle -i\vartheta|$. Finally, we have

$$
f_{nn'} = \sqrt{n'!n!}\sum_{\ell=0}^{n}\frac{(i\vartheta)^{n-\ell}(i\vartheta)^{n'-\ell}}{\ell!(n-\ell)!(n'-\ell)!}\langle -i\vartheta|0\rangle. \qquad \text{(A8)}
$$

The factor $\langle -i\vartheta|0\rangle$ can be calculated as

$$
\begin{aligned}
\langle -i\vartheta|0\rangle &= \langle 0|e^{ik_0 z}|0\rangle \\
&= \frac{1}{\sqrt{\pi m\omega_z}}\int dz e^{-m\omega_z z^2}e^{ik_0 z} \\
&= e^{-\frac{k_0^2}{4m\omega_z}} = e^{-\frac{1}{2}\vartheta^2}. \qquad \text{(A9)}
\end{aligned}
$$

The final result is

$$
f_{nn'} = \sqrt{n!n'!}\sum_{\ell=0}^{n}\frac{(i\vartheta)^{n-\ell}(i\vartheta)^{n'-\ell}}{\ell!(n-\ell)!(n'-\ell)!}e^{-\frac{1}{2}\vartheta^2}. \qquad \text{(A10)}
$$

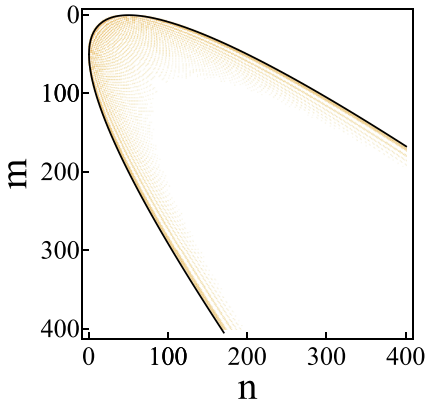

FIG. 6. $\vartheta = \sqrt{50}$ is fixed, and we show $|f_{mn}|^2$ more clearly by the matrix density diagram. Deep color means a nonzero value. As shown in the figure, when m and n are large, only a small number of points are nonzero, which behave like a dirac function. The black line is the result calculated by approximation (B6).

If $n' < n$, we find

$$
f_{nn'} = \sqrt{n!n'!}\sum_{\ell=0}^{n'}\frac{(i\vartheta)^{n-\ell}(i\vartheta)^{n'-\ell}}{\ell!(n-\ell)!(n'-\ell)!}e^{-\frac{1}{2}\vartheta^2}. \qquad \text{(A11)}
$$

In Fig. 6, we show the matrix element of $|f_{nn'}|$ as a function of n and n'. Meanwhile, in the main text, we approximate $|n\rangle$ as $\frac{1}{2}(|k_z\rangle \pm |-k_z\rangle)$, and then $f_{nn'} = \frac{1}{2}(\delta_{k_z',k_z+k_0} + \delta_{k_z',k_z-k_0})$. We show the solid line as the δ function between k_z and k_z'.

APPENDIX B: PREDICTIONS OF THE EFFECTIVE THEORY

Considering the fermions in a trap with the optical lattice in the x direction, the eigenstates are classified into two types. One type is the itinerate wave function and another is the localized one. When the excitation energy is above the mobility edge, then the localized eigenstate is labeled by its position in the x direction and n_z in the z direction. The energy of eigenstate $|j,n_z\rangle$ is

$$
\epsilon_{j,n_z} = \tfrac{1}{2}m\omega_x^2(ja_0)^2 + n_z\omega_z, \qquad \text{(B1)}
$$

where $a_0 = \pi/k_0$ is the lattice length unit. On the other hand, if the eigenenergy is smaller than the mobility edge, then we can approximate the excited-state energy by the local density approximation. $\epsilon_{j,k_x,n_z} = \frac{1}{2}m\omega_x^2(ja_0)^2 + n_z\omega_z + 2t\cos(k_x a_0)$, where t is the hopping strength in the x direction. From this dispersion relation, we can obtain the relation between the chemical potential and the particle number $N_{\rm at}$. Here we are going to focus on the case when the localized states are the major states (this is true when $N_{\rm at}$ is large):

$$
\begin{aligned}
N_{\rm at} &= \sum_{j,n_z} n_F(\epsilon_{j,n_z} - \mu) \\
&= \frac{2}{a_0}\int_0^{\sqrt{\frac{2\mu}{m\omega_x^2}}} dx \int_0^{\frac{\mu-\frac{1}{2}m\omega_x x^2}{\omega_z}} dn_z \\
&= \frac{4}{3\pi\omega_x\omega_z}\sqrt{\frac{2k_0^2}{m}}\mu^{3/2}. \qquad \text{(B2)}
\end{aligned}
$$

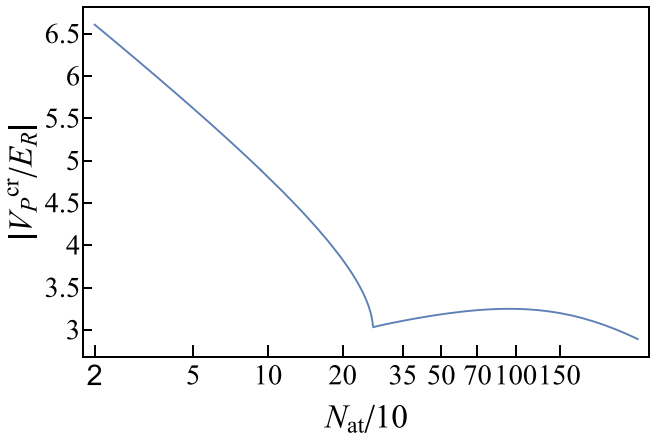

FIG. 7. We show $|V_P^{cr}(N_{at})/E_R|$ more clearly by this figure, from the above calculation, we can see that the shape of this universal curve is independent of ω_z, ω_x, and Δ_c'.

In above, we use $\sum_{j=-J}^{j=J} = \frac{1}{a_0}\int_{-Ja_0}^{Ja_0} dx$. Then we can see $\mu \propto N_{at}^{2/3}$. More explicitly,

$$\mu = \left(\frac{3\pi\omega_x\omega_z}{8\sqrt{E_R}}N_{at}\right)^{2/3}. \tag{B3}$$

Now we are going to check the critical pumping strength as a function of the chemical potential μ, and then equivalently we get the critical pumping strength as a function of N_{at} from the above relation. From Eq. (10), we know

$$\left|\frac{V_P^{cr}(N_{at})}{E_R}\right| = \frac{-\left(\Delta_c'^2+\kappa^2\right)E_R}{4U_0\Delta_c'\chi(N_{at})}, \tag{B4}$$

where the susceptibility χ is

$$\chi = \frac{1}{2\eta_0^2}\sum_{n,n'}\left|\int d\mathbf{r}\phi_n^*(\mathbf{r})\phi_{n'}(\mathbf{r})\eta(\mathbf{r})\right|^2\frac{n_F(E_n)-n_F(E_n')}{E_{n'}-E_n}. \tag{B5}$$

Note that the quantum number n represents all the quantum numbers of the eigenstate, including j, k_x, and n_z. Inspired by the asymptotic representation of hermite polynomials, $H_{2n_z}(z) = (-1)^{n_z}2^{n_z}(2n_z-1)!!e^{z^2/2}[\cos(\sqrt{4n_z+1}z)+O(\frac{1}{n_z^{1/4}})]$ and $H_{2n_z+1}(z) = (-1)^{n_z}2^{n_z+1/2}(2n_z-1)!!e^{z^2/2}\sqrt{2n_z+1}[\sin(\sqrt{4n_z+3}z)+O(\frac{1}{n_z^{1/4}})]$, we can take following approximations for large n_z,

$$\begin{aligned}\langle z|2n_z\rangle &\approx \frac{1}{2\sqrt{L_{k_z}}}(\langle z|k_z\rangle+\langle z|-k_z\rangle)\theta\left(L_{k_z}^2-z^2\right),\\ \langle z|2n_z+1\rangle &\approx \frac{1}{2\sqrt{L_{k_z}}}\left(\langle z|k_z\rangle-\langle z|-k_z\rangle\right)\theta\left(L_{k_z}^2-z^2\right)(k_z>0),\end{aligned} \tag{B6}$$

where $|k_z\rangle$ is a momentum state $\langle z|k_z\rangle = e^{ik_z z}$, $L_{k_z} = \frac{\pi|k_z|}{4m\omega_z}$, and $k_z^2/2m = n_z\omega_z$. The range in the z direction is due to the wave function being only obviously nonzero within the trap range. Here the plus sign is for n_z being even and the minus sign is for n_z being odd. This approximation is good when n_z is large, but we take this approximation for all n_z. Under such an approximation, we have

$$\begin{aligned}\langle 2n_z|e^{ik_0 z}|2n_z'\rangle = &\frac{1}{4\sqrt{L_{k_z}L_{k_z'}}}\int_{-\min(L_{k_z},L_{k_z'})}^{\min(L_{k_z},L_{k_z'})}\\ &\times dz(\langle k_z|+\langle -k_z|)|z\rangle e^{ik_0 z}\langle z|(|k_z'\rangle+|-k_z'\rangle).\end{aligned} \tag{B7}$$

Let us denote $L_{z\min} = \min(L_{k_z}, L_{k_z'})$ and $L_{z\max} = \max(L_{k_z}, L_{k_z'})$. Then we have

$$\begin{aligned}\langle 2n_z|e^{ik_0 z}|2n_z'\rangle = &\frac{\sin((k_0+k_z'-k_z)L_{z\min})}{(k_0+k_z'-k_z)(2\sqrt{L_{z\max}L_{z\min}})}+\frac{\sin((k_0+k_z'+k_z)L_{z\min})}{(k_0+k_z'+k_z)(2\sqrt{L_{z\max}L_{z\min}})}\\ &+\frac{\sin((k_0-k_z'-k_z)L_{z\min})}{(k_0-k_z'-k_z)(2\sqrt{L_{z\max}L_{z\min}})}+\frac{\sin((k_0-k_z'+k_z)L_{z\min})}{(k_0-k_z'+k_z)(2\sqrt{L_{z\max}L_{z\min}})}.\end{aligned} \tag{B8}$$

Notice that in the $\omega_z\to 0^+$ limit, $L_{z\min}\to\infty$, such that $\sin(kL_{z\min})/k \approx \delta(k)$. It is easy to check that $\langle 2n_z|e^{-ik_0 z}|2n_z'\rangle = \langle 2n_z|e^{ik_0 z}|2n_z'\rangle$, $\langle 2n_z|\cos(k_0 z)|2n_z'+1\rangle = \langle 2n_z+1|\cos(k_0 z)|2n_z'\rangle = 0$, and $\langle 2n_z+1|e^{ik_0 z}|2n_z'+1\rangle = \langle 2n_z+1|e^{-ik_0 z}|2n_z'+1\rangle$. What we really need is $|\langle 2n_z|e^{ik_0 z}|2n_z'\rangle|^2$; we have

$$\begin{aligned}\left|\langle 2n_z|\cos(k_0 z)|2n_z'\rangle\right|^2 &= (\langle 2n_z|e^{ik_0 z}|2n_z'\rangle)^2\\ &\approx \left(\frac{\sin[(k_0+k_z'-k_z)L_{z\min}]}{(k_0+k_z'-k_z)(2\sqrt{L_{z\max}L_{z\min}})}\right)^2+\left(\frac{\sin[(k_0+k_z'+k_z)L_{z\min}]}{(k_0+k_z'+k_z)(2\sqrt{L_{z\max}L_{z\min}})}\right)^2\\ &\quad+\left(\frac{\sin[(k_0-k_z'-k_z)L_{z\min}]}{(k_0-k_z'-k_z)(2\sqrt{L_{z\max}L_{z\min}})}\right)^2+\left(\frac{\sin[(k_0-k_z'+k_z)L_{z\min}]}{(k_0-k_z'+k_z)(2\sqrt{L_{z\max}L_{z\min}})}\right)^2\\ &\approx \left(\delta_{k_z,k_z'+k_0}+\delta_{-k_z,k_z'+k_0}+\delta_{k_z,-k_z'+k_0}+\delta_{-k_z,k_z'+k_0}\right)/(4L_{z\max}).\end{aligned} \tag{B9}$$

In the first $\approx$ in the above equation, we dropped the cross terms. In the second $\approx$, we employed $\lim_{L_{z\min}\to\infty}[\sin(kL_{z\min})/k]^2 \approx L_{z\min}\delta(k)$. Meanwhile when we replace $n_z\omega_z$ by $k_z^2/2m$, the summation over n_z is replaced by

$$\sum_{n_z} = \int_0^\infty dk_z \frac{k_z}{m\omega_z}. \tag{B10}$$

By approximation all the eigenstates are localized, and the susceptibility can be written as

$$\begin{aligned}
\chi(\mu) &= \frac{1}{2}\sum_{j,n_z;j',n_z'} \frac{|\langle j,n_z|\cos(k_0 z)\cos(k_0 x)|j',n_z'\rangle|^2}{\epsilon_{j,n_z}-\epsilon_{j',n_z'}}[\theta(\mu-\epsilon_{j',n_z'})-\theta(\mu-\epsilon_{j,n_z})] \\
&= \frac{1}{2}\sum_{\epsilon_{j',n_z'}\langle\mu,\epsilon_{j,n_z}\rangle\mu} \frac{|\langle j,n_z|\cos(k_0 z)\cos(k_0 x)|j',n_z'\rangle|^2}{\epsilon_{j,n_z}-\epsilon_{j',n_z'}} + \frac{1}{2}\sum_{\epsilon_{j',n_z'}>\mu,\epsilon_{j,n_z}<\mu} \frac{|\langle j,n_z|\cos(k_0 z)\cos(k_0 x)|j',n_z'\rangle|^2}{\epsilon_{j,n_z}-\epsilon_{j',n_z'}} \\
&= \sum_{\epsilon_{j',n_z'}>\mu,\epsilon_{j,n_z}<\mu} \frac{|\langle n_z|\cos(k_0 z)|n_z'\rangle|^2|\langle j|\cos(k_0 x)|j'\rangle|^2}{\epsilon_{j',n_z'}-\epsilon_{j,n_z}} = \sum_{\epsilon_{j,n_z}<\mu;n_z'} \frac{|\langle n_z|\cos(k_0 z)|n_z'\rangle|^2}{\epsilon_{j,n_z'}-\epsilon_{j,n_z}}\theta(\epsilon_{j,n_z'}-\mu).
\end{aligned} \tag{B11}$$

Where $|j\rangle$ represents the state localized in the jth site, now we introduce $x = ja_0$. Then $\sum_j = \frac{1}{a_0}\int dx$. In these approximations,

$$\begin{aligned}
\chi(\mu) &= \frac{1}{a_0}\int_{-\sqrt{\frac{2\mu}{m\omega_x^2}}}^{\sqrt{\frac{2\mu}{m\omega_x^2}}} dx \int_{-\sqrt{2m(\mu-1/2m\omega_x^2x^2)}}^{\sqrt{2m(\mu-1/2m\omega_x^2x^2)}} \frac{|k_z|dk_z}{2m\omega_z}\int \frac{|k_z'|dk_z'}{2m\omega_z}\frac{|\langle n_z|\cos(k_0 z)|n_z'\rangle|^2}{(n_z'-n_z)\omega_z}\theta\left(n_z'\omega_z+\frac{m\omega_x x^2}{2}-\mu\right) \\
&= \frac{1}{a_0}\int_{-\sqrt{\frac{2\mu}{m\omega_x^2}}}^{\sqrt{\frac{2\mu}{m\omega_x^2}}} dx \int_{-\sqrt{2m(\mu-1/2m\omega_x^2x^2)}}^{\sqrt{2m(\mu-1/2m\omega_x^2x^2)}} \frac{dk_z|k_z|}{2m\omega_z}\int \frac{|k_z'|dk_z'}{2m\omega_z}\frac{\left(\delta_{k_z,k_z'-k_0}+\delta_{k_z,-k_z'-k_0}+\delta_{-k_z,k_z'-k_0}+\delta_{-k_z,-k_z'-k_0}\right)}{4L_{z\max}\left(k_z'^2/2m-k_z^2/2m\right)} \\
&\quad\times\theta\left(\frac{k_z'^2}{2m}+\frac{m\omega_x^2x^2}{2}-\mu\right) \\
&= \frac{1}{a_0}\int_{-\sqrt{\frac{2\mu}{m\omega_x^2}}}^{\sqrt{\frac{2\mu}{m\omega_x^2}}} dx \int_{-\sqrt{2m(\mu-1/2m\omega_x^2x^2)}}^{\sqrt{2m(\mu-1/2m\omega_x^2x^2)}} \frac{|k_z|dk_z}{2m\omega_z}\int \frac{|k_z'|dk_z'}{2\pi\max(|k_z|,|k_z'|)} \\
&\quad\times\frac{\left(\delta_{k_z,k_z'-k_0}+\delta_{k_z,-k_z'-k_0}+\delta_{-k_z,k_z'-k_0}+\delta_{-k_z,-k_z'-k_0}\right)}{(k_z'^2/2m-k_z^2/2m)}\theta\left(\frac{k_z'^2}{2m}+\frac{m\omega_x^2x^2}{2}-\mu\right) \\
&= \frac{1}{a_0}\int_{-\sqrt{\frac{2\mu}{m\omega_x^2}}}^{\sqrt{\frac{2\mu}{m\omega_x^2}}} dx \int_{-\sqrt{2m(\mu-1/2m\omega_x^2x^2)}}^{\sqrt{2m(\mu-1/2m\omega_x^2x^2)}} \frac{|k_z|dk_z}{2m\omega_z}\frac{|k_z+k_0|}{2\pi\max(|k_z|,|k_z+k_0|)}\frac{\theta\left(\frac{(k_z+k_0)^2}{2m}+\frac{m\omega_x^2x^2}{2}-\mu\right)}{(k_z+k_0)^2/2m-k_z^2/2m} \\
&\quad+\frac{1}{a_0}\int_{-\sqrt{\frac{2\mu}{m\omega_x^2}}}^{\sqrt{\frac{2\mu}{m\omega_x^2}}} dx \int_{-\sqrt{2m(\mu-1/2m\omega_x^2x^2)}}^{\sqrt{2m(\mu-1/2m\omega_x^2x^2)}} \frac{|k_z|dk_z}{2m\omega_z}\frac{|k_z+k_0|}{2\pi\max(|k_z|,|k_z+k_0|)}\frac{\theta\left(\frac{(k_z+k_0)^2}{2m}+\frac{m\omega_x^2x^2}{2}-\mu\right)}{(k_z+k_0)^2/2m-k_z^2/2m} \\
&\quad+\frac{1}{a_0}\int_{-\sqrt{\frac{2\mu}{m\omega_x^2}}}^{\sqrt{\frac{2\mu}{m\omega_x^2}}} dx \int_{-\sqrt{2m(\mu-1/2m\omega_x^2x^2)}}^{\sqrt{2m(\mu-1/2m\omega_x^2x^2)}} \frac{|k_z|dk_z}{2m\omega_z}\frac{|k_z-k_0|}{2\pi\max(|k_z|,|k_z-k_0|)}\frac{\theta\left(\frac{(k_z-k_0)^2}{2m}+\frac{m\omega_x^2x^2}{2}-\mu\right)}{(k_z-k_0)^2/2m-k_z^2/2m} \\
&\quad+\frac{1}{a_0}\int_{-\sqrt{\frac{2\mu}{m\omega_x^2}}}^{\sqrt{\frac{2\mu}{m\omega_x^2}}} dx \int_{-\sqrt{2m(\mu-1/2m\omega_x^2x^2)}}^{\sqrt{2m(\mu-1/2m\omega_x^2x^2)}} \frac{|k_z|dk_z}{2m\omega_z}\frac{|k_z-k_0|}{2\pi\max(|k_z|,|k_z-k_0|)}\frac{\theta\left(\frac{(k_z-k_0)^2}{2m}+\frac{m\omega_x^2x^2}{2}-\mu\right)}{(k_z-k_0)^2/2m-k_z^2/2m} \\
&= \frac{2}{a_0}\int_{-\sqrt{\frac{2\mu}{m\omega_x^2}}}^{\sqrt{\frac{2\mu}{m\omega_x^2}}} dx \int_{-\sqrt{2m(\mu-1/2m\omega_x^2x^2)}}^{\sqrt{2m(\mu-1/2m\omega_x^2x^2)}} \frac{|k_z|dk_z}{2m\omega_z}\frac{|k_z+k_0|}{2\pi\max(|k_z|,|k_z+k_0|)}\frac{\theta\left(\frac{(k_z+k_0)^2}{2m}+\frac{m\omega_x^2x^2}{2}-\mu\right)}{(k_z+k_0)^2/2m-k_z^2/2m} \\
&\quad+\frac{2}{a_0}\int_{-\sqrt{\frac{2\mu}{m\omega_x^2}}}^{\sqrt{\frac{2\mu}{m\omega_x^2}}} dx \int_{-\sqrt{2m(\mu-1/2m\omega_x^2x^2)}}^{\sqrt{2m(\mu-1/2m\omega_x^2x^2)}} \frac{|k_z|dk_z}{2m\omega_z}\frac{|k_z-k_0|}{2\pi\max(|k_z|,|k_z-k_0|)}\frac{\theta\left(\frac{(k_z-k_0)^2}{2m}+\frac{m\omega_x^2x^2}{2}-\mu\right)}{(k_z-k_0)^2/2m-k_z^2/2m}.
\end{aligned}$$

Notice that when we change k_z to $-k_z$ the integral function does not change, so we just need to consider $k_z > 0$:

$$\chi(\mu) = \frac{8}{a_0}\int_0^{\sqrt{\frac{2\mu}{m\omega_x^2}}} dx \int_0^{\sqrt{2m(\mu-1/2m\omega_x^2x^2)}} \frac{k_z dk_z}{2m\omega_z} \frac{k_z+k_0}{2\pi \max(\mathrm{k_z}, \mathrm{k_z}+\mathrm{k_0})} \frac{\theta\left(\frac{(k_z+k_0)^2}{2m}+\frac{m\omega_x^2x^2}{2}-\mu\right)}{(k_z+k_0)^2/2m - k_z^2/2m}$$
$$+ \frac{8}{a_0}\int_0^{\sqrt{\frac{2\mu}{m\omega_x^2}}} dx \int_0^{\sqrt{2m(\mu-1/2m\omega_x^2x^2)}} \frac{k_z dk_z}{2m\omega_z} \frac{|k_z-k_0|}{2\pi \max(\mathrm{k_z}, |\mathrm{k_z}-\mathrm{k_0}|)} \frac{\theta\left(\frac{(k_z-k_0)^2}{2m}+\frac{m\omega_x^2x^2}{2}-\mu\right)}{(k_z-k_0)^2/2m - k_z^2/2m}.$$

The calculation is carried out in the following three cases: $\mu/E_R < 1/4$, $1/4 < \mu/E_R < 1$, and $\mu/E_R \gg 1$.

For $\mu < 1/4E_R$, the θ function in χ is always satisfied:

$$\chi(\mu) = \frac{4\sqrt{\mu E_R}}{\pi^2\omega_z\omega_x}\left[-1+1\sqrt{-1+\frac{E_R}{4\mu}}\arctan\left(1/\sqrt{-1+\frac{E_R}{4\mu}}\right)\right]. \tag{B12}$$

For $1/4 < \mu/E_R < 1$,

$$\chi(\mu) = \frac{-4\mu}{\pi^2\omega_x\omega_z}\left[0.5\sin\left(2\arcsin\sqrt{1-\frac{E_R}{4\mu}}\right)+\arcsin\sqrt{1-\frac{E_R}{4\mu}}\right] + \frac{4}{\pi^2\omega_x\omega_z}\sqrt{E_R\mu}\sqrt{1-\frac{E_R}{4\mu}}$$
$$+ \frac{2\sqrt{E_R\mu}}{\omega_x\omega_z\pi^2}\left[-2-\sqrt{1-\frac{E_R}{4\mu}}\log\left(\frac{1-\sqrt{1-\frac{E_R}{4\mu}}}{1+\sqrt{1-\frac{E_R}{4\mu}}}\right)\right]. \tag{B13}$$

For $\mu \gg E_R$,

$$\chi(\mu) \approx \frac{4}{\pi^2\omega_x\omega_z}\sqrt{\mu E_R}. \tag{B14}$$

Apply critical condition $\Delta_c' + 4\chi\Delta_c'^2/(\Delta_c'^2+\kappa^2) = 0$, and we get

$$\left|V_P^{\mathrm{cr}}/E_R\right| \approx \frac{\Delta_c'^2+\kappa^2}{16\Delta_c' U_0}\left(\pi^2\omega_x\omega_z/E_R^2\right)\left(\frac{3\pi\omega_x\omega_z}{8E_R^2}N_{\mathrm{at}}\right)^{-\frac{1}{3}} \propto N_{\mathrm{at}}^{-1/3}. \tag{B15}$$

In Fig. 7, we show the critical pumping strength as a function of atom number N_{at} by Eq. (B4) and the susceptibility given by Eq. (B11).

[1] F. Brennecke, T. Donner, S. Ritter, T. Bourdel, M. Köhl, and T. Esslinger, Nature (London) **450**, 268 (2007).
[2] Y. Colombe, T. Steinmetz, G. Dubios, F. Linke, D. Hunger, and J. Reichel, Nature (London) **450**, 272 (2007).
[3] K. Baumann, C. Guerlin, F. Brennecke, and T. Esslinger, Nature (London) **464**, 1301 (2010).
[4] R. H. Dicke, Phys. Rev. **93**, 99 (1954).
[5] K. Hepp and E. H. Lieb, Ann. Phys. **76**, 360 (1973).
[6] K. Baumann, R. Mottl, F. Brennecke, and T. Esslinger, Phys. Rev. Lett. **107**, 140402 (2011).
[7] R. Mottl, F. Brennecke, K. Baumann, R. Landig, T. Donner, and T. Esslinger, Science **336**, 1570 (2012).
[8] F. Brennecke, R. Mottl, K. Baumann, R. Landig, T. Donner, and T. Esslinger, Proc. Natl. Acad. Sci. USA **110**, 11763 (2013).
[9] J. Klinder, H. Keßler, M. Wolke, L. Mathey, and A. Hemmerich, Proc. Natl. Acad. Sci. USA **112**, 3290 (2015).
[10] R. Landig, F. Brennecke, R. Mottl, T. Donner, and T. Esslinger, Nat. Commun. **6**, 7046 (2015).
[11] J. Klinder, H. Keßler, M. R. Bakhtiari, M. Thorwart, and A. Hemmerich, Phys. Rev. Lett. **115**, 230403 (2015).
[12] R. Landig, L. Hruby, N. Dogra, M. Landini, R. Mottl, T. Donner, and T. Esslinger, Nature (London) **532**, 476 (2016).
[13] L. Hruby, N. Dogra, M. Landini, T. Donner, and T. Esslinger, Proc. Natl. Acad. Sci. USA **115**, 3279 (2018).
[14] X. Li, D. Dreon, P. Zupancic, A. Baumgartner, A. Morales, W. Zheng, N. R. Cooper, T. Donner, and T. Esslinger, Phys. Rev. Res. **3**, L012024 (2021).
[15] J. Léonard, A. Morales, P. Zupancic, T. Esslinger, and T. Donner, Nature (London) **543**, 87 (2017).
[16] J. Léonard, A. Morales, P. Zupancic, T. Donner, and T. Esslinger, Science **358**, 1415 (2017).
[17] A. Morales, P. Zupancic, J. Léonard, T. Esslinger, and T. Donner, Nat. Mater. **17**, 686 (2018).
[18] F. Mivehvar, F. Piazza, T. Donner, and H. Ritsch, Ann. Phys. **70**, 1 (2021).
[19] J. Keeling, M. J. Bhaseen, and B. D. Simons, Phys. Rev. Lett. **112**, 143002 (2014).
[20] F. Piazza and P. Strack, Phys. Rev. Lett. **112**, 143003 (2014).
[21] Y. Chen, Z. Yu, and H. Zhai, Phys. Rev. Lett. **112**, 143004 (2014).

[22] Y. Chen, H. Zhai, and Z. Yu, Phys. Rev. A **91**, 021602(R) (2015).
[23] X. Zhang, Y. Chen, Z. Wu, J. Wang, J. Fan, S. Deng, and H. Wu, Science **373**, 1359 (2021).
[24] V. Helson, T. Zwettler, F. Mivehvar, E. Colella, K. Roux, H. Konishi, H. Ritsch, and J.-P. Brantut, Nature (London) **618**, 716 (2023).
[25] Y. Margalit, Y.-K. Lu, F. C. Top, and W. Ketterle, Science **374**, 976 (2021).
[26] A. B. Deb and N. Kjærgaard, Science **374**, 972 (2021).
[27] C. Sanner, L. Sonderhouse, R. B. Hutson, L. Yan, W. R. Milner, and J. Ye, Science **374**, 979 (2021).
[28] J. S. Pan, X. J. Liu, W. Zhang, W. Yi, and G. C. Guo, Phys. Rev. Lett. **115**, 045303 (2015).
[29] See the Appendices for the details. In the Appendices, we include the calculations for the off-diagonal matrix element $\langle n|\cos(k_0 z)|n'\rangle$ and the results for an approximate field theory.